

ALMA memo No. 574

Design of the central cone for the subreflector of the ACA 7-m antenna

Masahiro SUGIMOTO¹, Junji INATANI¹,
Baltasar VILA-VILARO¹, Masao SAITO¹,
and Satoru IGUCHI¹

¹*ALMA project office, National Astronomical Observatory of Japan,
2-21-1 Osawa Mitaka Tokyo 181-8588, Japan
masahiro.sugimoto@nao.ac.jp*

2007-11-13

Abstract

We have designed the central cone for the subreflector of the ACA 7-m antenna. The cone is curved-shape and 53 mm in diameter, which is the maximum size to the extent that the cone does not affect the efficiency of the antenna even at the highest frequency of ALMA, 950 GHz. We have also optimized the profile parameters of the cone in consideration of off-axis feeds, especially for the lower frequency bands, so that the electric field reflected by the subreflector will be well suppressed within a radius of the vertex hole on the Cassegrain focal plane.

According to our analysis, tilting the subreflector is effective to reduce the efficiency loss and the spillover for the main reflector. Since the same type of receivers will be used on both the 7-m and 12-m antennas, the subreflector of the 7-m antenna should be tilted more than that of the 12-m antenna. We have compared the cases of a non-ideal subreflector tilt angle (1.215 degrees, i.e., the maximum tilt angle for the 12-m subreflector) and an ideal tilt angle for the reference to mechanical design of the 7-m antenna. The difference in performance between these cases was remarkable especially in Band 5–6, however, no serious performance degradations were found.

Key words: instrumentation: optics — antenna, receiver, millimeter/submillimeter

1. Introduction

The Atacama Compact Array (ACA) consists of sixteen antennas (twelve 7-m antennas for the interferometry and four 12-m antennas for the total power measurements), aiming to im-

prove the short baseline coverage of ALMA observations, especially for extended astronomical sources. Various studies have been conducted for ACA about the element antenna, its configuration, and imaging capability (e.g. Baars 2000; Pety, Gueth, & Guilloteau 2001; Tsutsumi et al. 2004; Morita & Holdway 2005). The ACA 12-m antenna shares the optics parameters with the 12-m antenna used for ALMA which is comprised of sixty four 12-m antennas. The design for the central cone of the subreflector (Lamb 1999, Hills 2005) for both ACA 12-m antenna and ALMA is also identical.

The electromagnetic design of the central cone was first studied for the 12-m antenna by Bacmann (2003). The result showed that the cone was effective to reduce the standing waves between the feed and the subreflector, and suggested that a cone should be 1.1 to 1.2 times larger than the geometrically blocked area (i.e., the central area of the subreflector surface that is not hit by the incident rays from the sky). The design was developed in detail by Hills (2005) in consideration of the effect of the feed offset and the sensitivity.

To optimize the central cone, two aspects should be taken into account: (1) to reduce the amplitude of the reflection from the subreflector to the feed (the highest priority and the main reason to introduce the cone), and (2) to prevent the sensitivity degradation and to maximize the sensitivity if possible. When using the subreflector without a cone, the reflection amplitude to couple with the feed is generally proportional to wavelength. Even with a cone, the reflected field is not effectively suppressed in the lower frequency range. It is also concerned that the area of low reflected power on the Cassegrain focal plane will be narrow if the feeds have large offset like ALMA. According to these facts, the millimeter wavelength should be studied more closely than the submillimeter wavelength in order to realize the aspect (1) mentioned above. As for the aspect (2), we need to decide the frequency for which the cone should be optimized based on how the antenna is used. This is because the proper size and shape of the cone is different in frequency. If we compare G/T at 950 GHz and 100 GHz, a rough estimation shows that G/T at 950 GHz is twice larger than that at 100 GHz (we assumed the antenna gain, $G = 4\pi A_e/\lambda^2$ where A_e is effective aperture which is proportional to Ruze loss with 20 μm rms, and $T_{\text{sys}} = 1200$ K and 50 K for each frequency). This estimation suggests that the cone should be optimized for the low frequency. This is appropriate for observation of point sources smaller than the beam size, but not for ACA which mainly observes extended celestial objects. As for ACA, it is proper to use aperture efficiency, ϵ_{ap} , instead of the antenna gain. With the aperture efficiency, the calculation shows that ϵ_{ap}/T at 950 GHz is as low as one fiftieth of that at 100 GHz (2:100 in ratio). Since the sensitivity in the high frequency is absolutely low, we do not want to further reduce it by optimizing the cone for the low frequency. Therefore, we conclude that we should optimize the cone in high frequency.

There is another difficulty to deal with the size of the cone. The power reflected toward the feed generally decreases as the size of the cone increases. On the other hand, the cone larger than the geometrical blockage has a possibility to reduce the sensitivity because the area

around the vertex hole of the primary may not be used effectively. Thus, if the cone cannot comply with our requirement of the aspect (1), we have to enlarge the cone size, giving up maximizing the sensitivity of the aspect (2).

This memo describes the design of the central cone for the ACA 7-m antenna and its performance. Based on the above background, we optimized the cone size to avoid the loss of the efficiency even at 950 GHz and to maximize the sensitivity around this frequency range. The curved-shape cone was introduced to well suppress the reflection amplitude, which is comparable with those of 12-m antenna. Firstly, the optics parameters of the ACA 7-m antenna are briefly described in Section 2. In Section 3, the calculation methods and definitions of the parameters are presented. With those methods, the diameter of the cone is optimized and its performance is shown in Section 4.

2. Antenna Optics Parameters

Figure 1 shows the definition of optics parameters tabulated in Table 1. All calculations in this memo are based on those parameters for the ACA 7-m antenna. Basic assumptions for the calculations are:

- The half angle subtended by the subreflector radius seen from the Cassegrain focus is equivalent with that of the 12-m antenna ($\phi_s = 3^\circ 58'$, Lamb 1999).
- The diameter of the vertex hole is equivalent to that of the 12-m antenna (i.e., 750 mm).
- The physical diameter of the subreflector required to cover the hyperboloid mirror and its outer skirt region is regarded as equivalent with that of the vertex hole. The skirt shape will be optimized to reduce the ground pickup noise. However the skirt design is out of scope of this memo.

Figure 2 shows the schematic drawing of the antenna. The Cassegrain focus will be set around the elevation axis.

3. Calculation methods and definitions

3.1. Field profile, efficiency and spillover

To evaluate the effect of the subreflector central cone, it is essential to know the electric field distribution on the Cassegrain focal plane, or on the primary reflector surface, which is dependent on the receiver feed characteristics and its location as well as the subreflector shape and tilt angle. As described in Hills (2005), the scalar approximation of the Physical Optics (PO) is sufficient to calculate the field distribution. We adopted the method to save the calculation time. Details of the method are found in Hills (1986) and Zhang (1996). Firstly, we ran our program for cases of the 12-m antenna and checked whether it successfully gave fields consistent with those by Hills (2005). For the calculation of the efficiency, we basically used a software which performs the proper vector integration, taking account of currents on the

Table 1. Antenna optics parameters

Parameters	Abbreviation	12-m*	7-m
Primary mirror diameter	D_m	12000.000 mm	7000.000 mm
Primary focal length	F_m	4800.000 mm	2571.693 mm
Secondary Mirror Diameter	D_s	750.000 mm	456.892 mm
Vertex hole size	D_v	750.000 mm	750.000 mm
Focal length of the equivalent paraboloid	F_e	96000.000 mm	56000.000 mm
Primary focal ratio	F_m/D_m	0.40000	0.36738
Secondary focal ratio	F_e/D_m	8.00000	8.00000
Magnification	M	20.00000	21.77554
Half-angle subtended by the main dish	ϕ_m	64°01077	68°46944
Half-angle subtended by the subreflector	ϕ_s	3°5798	3°5798
Eccentricity	e	1.10526	1.09627
	a	2794.336 mm	1706.561 mm
Secondary mirror interfocal distance	$F_s(2c)$	6176.953 mm	3741.693 mm
	L_a	5994.141 mm	3651.565 mm
	L_b	182.813 mm	90.128 mm
Cass. focus to the subreflector	L_f	5882.813 mm	3577.407 mm
Primary focus to the subreflector	L_s	294.141 mm	164.286 mm
Depth of the main dish	X_m	1875.000 mm	1190.8497 mm
Depth of the subreflector	X_s	111.32813 mm	74.158 mm
Back focal distance	X_f	1376.953 mm	1170.000 mm
Distance between the primary vertex and EL axis	X_e	1931.000 mm	1150.000 mm
Height of the mechanical box from the primary focus	X_t	697.900 mm	653.307 mm
Close packing ratio	P_r	1.24	1.25

* Proto-type 12-m antenna made by the MELCO.

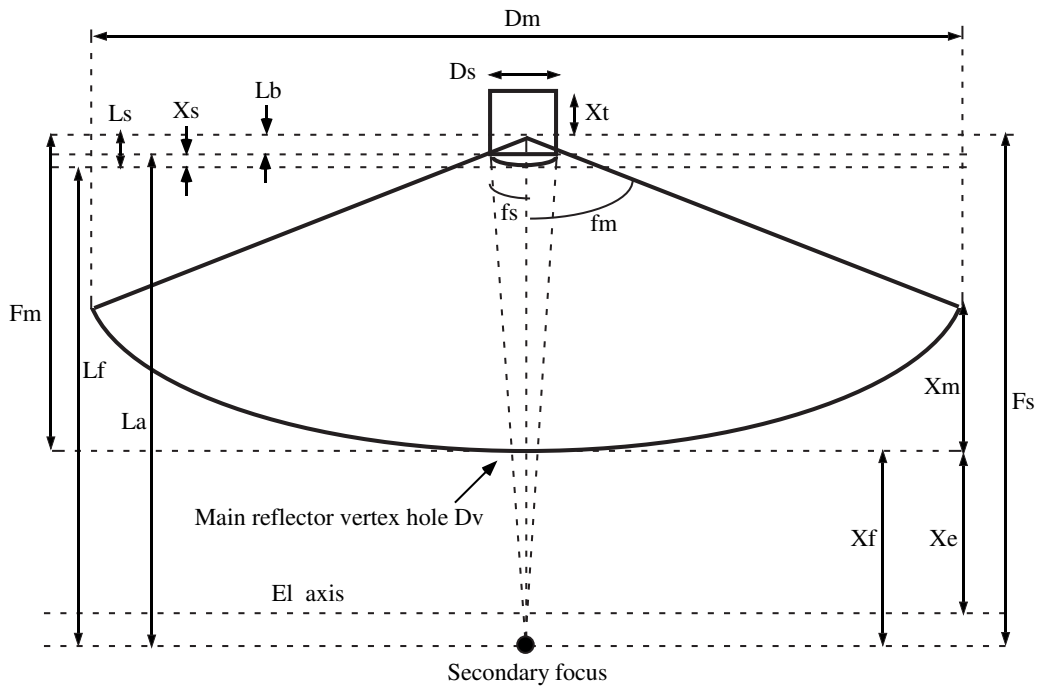


Fig. 1. Definition of the 7-m antenna optics parameters.

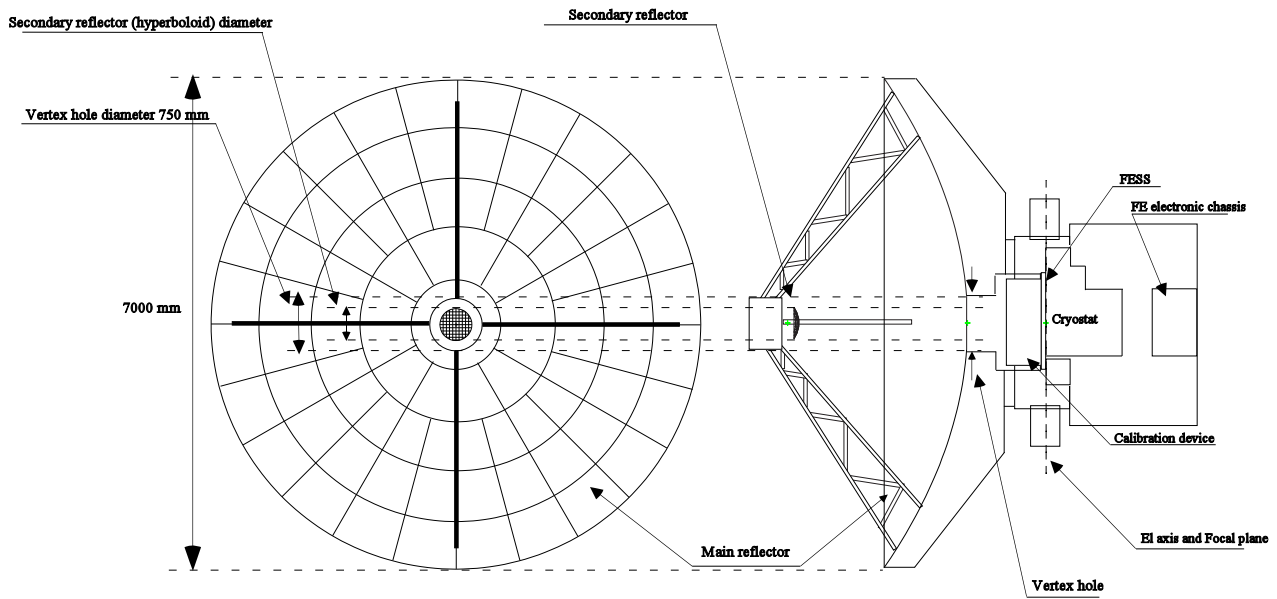


Fig. 2. Schematic drawing of the 7-m antenna mechanical structure.

reflectors, i.e. GRASP. For evaluation of the spillover loss at the primary reflector, we took the ratio of the total power hitting the primary to the spilled power, using the illumination profiles calculated by the scalar PO.

Figures 3 (a) and (b) show the cases of a complete subreflector with a hyperbolic profile (meaning the subreflector without a cone) for the ACA 7-m antenna. We have assumed a 100 GHz feed at the center of the focal plane (i.e., on-axis) with a Gaussian illumination and 12 dB edge taper at the subreflector. Black solid lines in (a) indicate the outer edge of the primary ($r = 3500$ mm) and that of the central vertex hole ($r = 375$ mm). The solid lines in (b) represent a clear aperture of 600 mm in diameter at the Cassegrain focal plane. We see the prominent features that were explained by Hills (2005); (1) the ripples which extend to the edge of the primary resemble the Fresnel diffraction pattern, and (2) the Poisson's spot at the center, which is attributed to the fact that the subreflector is completely circular and the all diffracted waves are added up in phase here. Figures 3 (c) and (d) show the case of suppressed Poisson's spot. This suppression was artificially introduced by making the ± 2 mm region of the outer edge fade out linearly. We conduct the artificial suppression hereafter to clearly demonstrate the effect of the cone.

3.2. Profile of curved cone

The curved cone can reduce the return power to the feed more effectively compared with the straight one (Padman and Hills 1991). For the 12-m antenna, Bacmann (2003) and Hills (2005) have indicated that a lower reflection is obtained with a slightly curved cone. The curved cone also generates low reflected power in a wider area on the Cassegrain focal plane. To optimize the curved cone, a polynomial profile with 4 terms was assumed as

$$dz = A + Bq + Cq^2 + Dq^3, \quad (1)$$

where

$$q = (r_c - r)/r_c, \quad (2)$$

dz is the axial deviation from the nominal hyperboloid, and r_c is the outer edge radius of the cone. As demonstrated by Hills (2005), the coefficients A and B were set to zero and only C and D were allowed to vary. Figure 4 describes the amplitude of the reflected field at the on-axis Cassegrain focus. The cone diameter was assumed to be 53 mm ($r_c = 26.5$ mm) in this calculation. The on-axis reflection is reduced when we chose the negative quantities for C and D. The lower right map in Figure 4 indicates the averaged amplitude for all frequencies (100, 150, 183, 230, and 270 GHz) in a focused range of C and D. Two minimum points can be found at $C = -0.19$, $D = -0.80$ (hereafter cone A) and at $C = -0.62$, $D = -1.36$ (cone B), respectively.

Figure 5 shows the amplitudes of the on-axis reflection with the cones, relative to that for a perfect hyperboloid (meaning the subreflector without any cone). The black line indicates

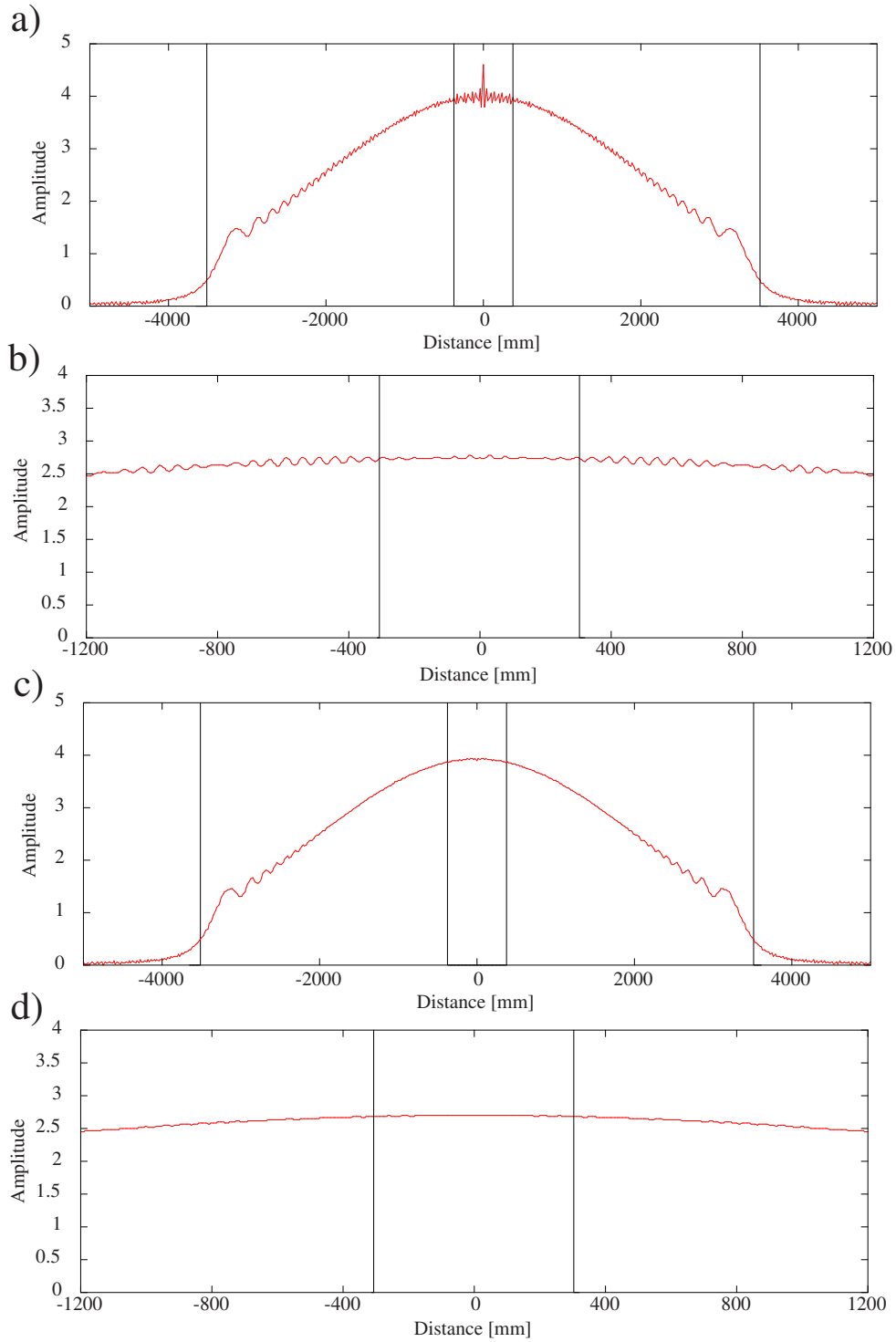


Fig. 3. (a) Illumination amplitude of the on the primary reflector calculated with a Gaussian beam at the subreflector with a 12 dB edge taper at 100 GHz. (b) The same as (a), but calculated on the Cassegrain focal plane. (c) The same as (a), but for the case that the subreflector illumination is faded out linearly in a 4 mm-wide region of its rim. (d) The same as (c), but calculated on the Cassegrain focal plane.

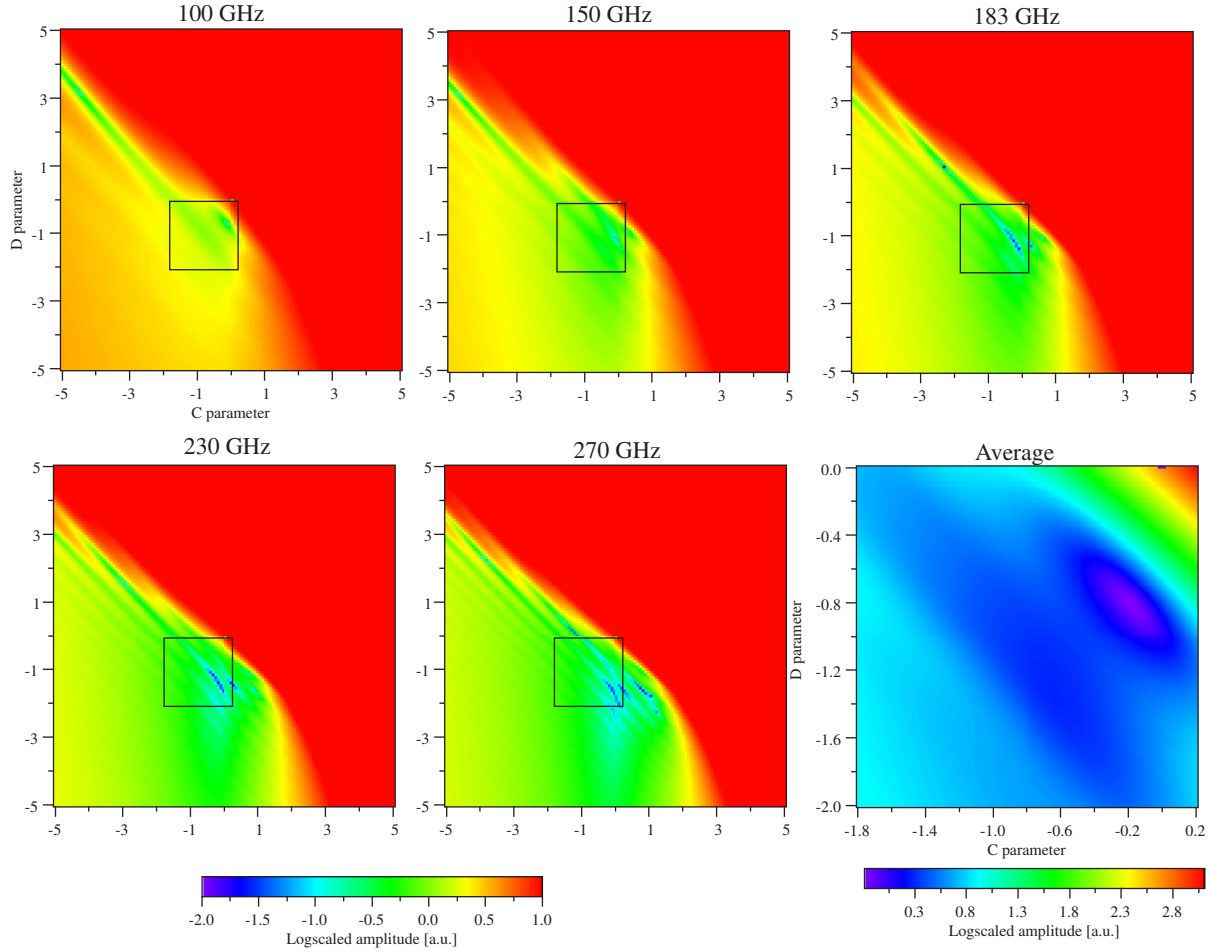


Fig. 4. Each map describes how the reflected field amplitude at the on-axis Cassegrain focus is dependent on the curved cone parameters C and D, for 100, 150, 183, 230, and 270 GHz. The x and y axes correspond to C and D in the equation (1).

a straight cone with a slope that matches the hyperbolic surface gradient at its outer edge. The blue and red lines represent the curved cone A and curved cone B. At 140 GHz and below, the cone B has slightly higher reflections than the curved cone A. The amplitude profiles of the reflected field on the Cassegrain focal plane at 100 GHz are shown in Figure 6. You can see the cone B generates lower reflection in a wider area while the reflection of the cone A is lower only on the axis. Thus we conclude that the cone B is more appropriate for the feed offset.

Figure 7 shows physical profiles for the straight cone, the cone A, and the cone B.

3.3. Reflection coefficient and peak-to-peak ripple

It is well known that multiple reflections in the optical path of a radiotelescope produce a quasi-sinusoidal modulation of the antenna gain, which is referred to as "standing waves" or "baseline ripple". To evaluate the effect caused by the reflection between the secondary and the feed, we define the ratio of the maximum peak-to-peak ripple to the nominal power level as

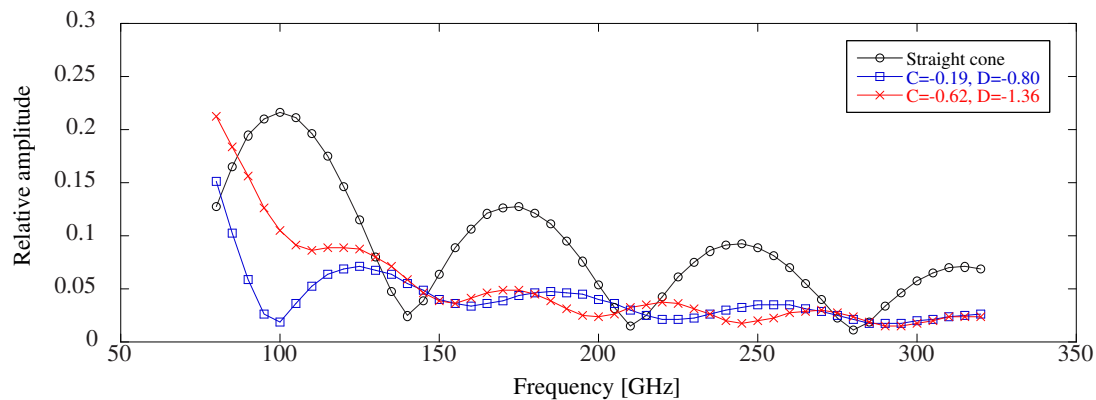


Fig. 5. Amplitude of the on-axis reflection with the cones relative to that for a smooth hyperboloid. The blue and red lines indicate the curved cones.

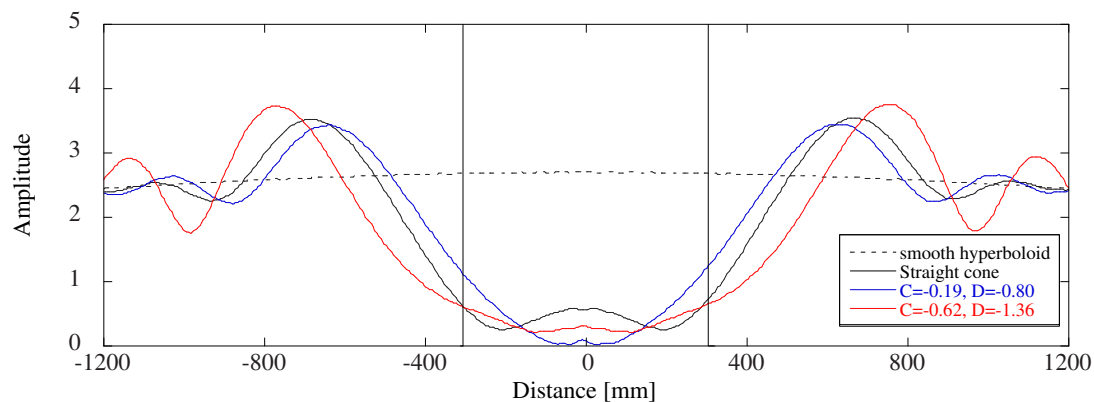


Fig. 6. Amplitude of the illumination on the Cassegrain plane at 100 GHz. The blue and red lines indicate the curved cone.

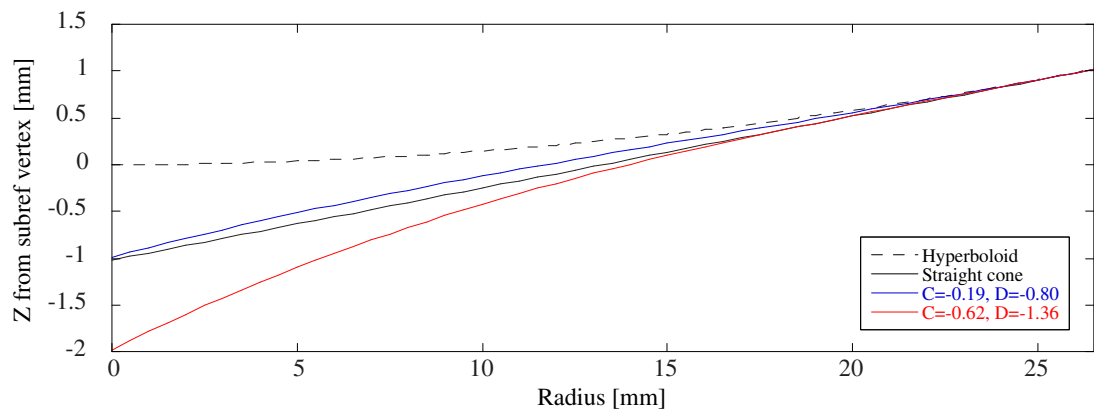


Fig. 7. The physical profile for the cones in different shapes. The blue and red lines indicate the curved cone.

$$\Delta P/P = 4\Gamma_s\Gamma_f, \quad (3)$$

where Γ_s and Γ_f are the reflection coefficients at the secondary and at the feed (Morris 1978, Bacmann 2003). The reflection coefficient at the secondary without the cone, Γ_{s0} , can be expressed as

$$\Gamma_{s0} = \frac{2\pi L_s w_0^2}{\lambda L_f (L_f + L_s)}, \quad (4)$$

where w_0 is the size of the beam waist at the feed (Lucke et al. 2005). The equation can be derived from the calculation of the coupling between the gaussian beam of the feed and the beam emitted by the virtual image at the primary focus. We have to note that the above equation was originally introduced by Lucke et al. (2005) for their calculation: the reflection coefficient expressed by the equation (4) is derived on condition that the secondary is infinitely extending. We adopted this equation here for simplicity. If we define the ratio of the amplitude reflected to the Cassegrain plane without the cone to that with the cone as a cone factor, η_{cone} (e.g., solid lines divided by the dash line in Figure 6), we can calculate the reflection coefficient for the subreflector with the cones as

$$\Gamma_s = \Gamma_{s0} \cdot \eta_{\text{cone}}. \quad (5)$$

We adopt $\Gamma_f = 0.4$ (-8 dB) hereafter as an assumed value.

For the ACA 7-m antenna, the frequency of the standing waves is expected to be $\nu = c/2L_f \sim 41.9$ MHz, where c is the speed of light.

4. The cone design

The most important function of the cone is to suppress the reflection power, which is related to the diameter size of the cone. The reflection power toward the Cassegrain focus generally decreases as the size of the cone increases. Therefore, the most effective way to suppress it, especially in low frequency ranges, is to enlarge the cone. From that viewpoint, the cones 1.1 to 1.3 times larger than the geometrically blocked area were proposed for the 12-m antenna. However the cone larger than the geometrical blockage has a possibility to diminish the aperture efficiency in the high frequency ranges by creating an extra non-illumination area surrounding the vertex hole. This is what we should avoid especially for the 7-m antenna because its gain is smaller than the 12-m antenna. We should consider the balance between suppression of the reflection power and guarantee of the efficiency when designing the cone.

To determine the diameter of the cone, we used the calculation of the sensitivity in Section 4.1. We selected the largest cone size that does not reduce the aperture efficiency even at 950 GHz with maximum sensitivity. In Section 4.2 the reflection performance including the effect of the feed offset is checked in the low frequency ranges.

4.1. Cone diameter

According to the ray-tracing results, a central area of the secondary ($\phi 47.9$ mm) optically corresponds to the vertex hole D_v , which is $\phi 750$ mm on the primary. The efficiency degradation due to the suppression on the primary center will be roughly estimated from

$$\eta_{bt} = \frac{[\exp(-f_b^2\alpha) - \exp(-\alpha)]^2}{[1 - \exp(-\alpha)]^2} \quad (6)$$

where α is 1.38 in 12 dB edge taper and f_b is the ratio of the shadow area's diameter to the primary's diameter (Goldsmith 1998). When the cone is 60 mm in diameter, for example, the corresponding shadow area on the primary is $\phi 940$ mm, and the degradation of the aperture efficiency is calculated to be -2.3 % from the equation (6). Based on the above estimation, we performed PO calculations for cones whose diameters are from 48 to 60 mm. The results are summarized in Table 2.

Table 2 indicates the relative aperture efficiency and the spillover at 950 GHz for the straight cones. The relative aperture efficiency, $\Delta\epsilon_{ap}$, represents a change in the aperture efficiency compared with the case without a cone. As for the spillover on the primary, two types are considered; the spillover into the vertex hole and the spillover going outside the primary. The relative sensitivity¹, $\Delta\epsilon_{ap}/T$, was calculated on condition that a spillover of 1 % terminated at ambient temperature adds 1.3 % to the system temperature, which is about right for a system temperature of 1200 K (see Appendix A). Figure 8 shows the illumination profiles on the primary and on the Cassegrain focal plane. The spillover into the vertex hole decreases rapidly as the diameter increases. For the 53 mm-diameter cone, the spillover into the vertex hole attains a level comparable to the spillover going outside the edge of the primary. In the case of the 60 mm cone, it generates a non-illumination area around the vertex hole on the primary ($r=375$ mm to 420 mm), which explains the efficiency degradation in Table 2.

It is interesting to see additional efficiencies associated with straight cones of smaller diameters (48 to 52 mm in Table 2). Details of the illumination profile on the primary will explain that reason. Figure 9 describes the amplitude on the primary surface and the phase on the aperture plane for the straight cone 50 mm in diameter. The power scattered by the cone has a sharp peak in the amplitude around $r=375$ mm. The phase seems to be distorted. It means that the waves scattered by the cone are partially added in phase, resulting in the additional efficiencies. When using the curved cone, such additional efficiencies are not guaranteed because the phase pattern seems significantly different from the case with the straight cone (e.g., Figure 7 shows that the difference between differently-shaped cones is comparable with or larger than the wavelength of 950 GHz). Figure 10 shows the amplitude and phase on the primary in the case of the curved cone B of 53 mm in diameter. The periodic ripples in the phase pattern seem

¹ Although $\Delta\epsilon_{ap}$ and $\Delta\epsilon_{ap}/T$ are practically equivalent to "Gain" and "G/T" defined in the table of Hills (2005) as far as we discuss relative changes of them at a fixed frequency, the different abbreviations are used to avoid readers' confusions as described in Section 1.

Table 2. Efficiency and Spillover for the straight cone at 950 GHz

Freq. [GHz]	Feed offset	Tilt of subref	Cone dia.	Spillover [%]			$\Delta\epsilon_{\text{ap}}$ [%]*	$\Delta\epsilon_{\text{ap}}/T$ [%]*
				into hole	outside the edge	Total		
950	On axis	None	None	3.35	0.11	3.46	0.00	0.00
			48 mm	2.85	0.11	2.96	0.38	1.04
			50 mm	1.59	0.11	1.70	0.88	3.25
			52 mm	0.38	0.11	0.49	0.49	4.53
			53 mm	0.16	0.11	0.27	0.06	4.40
			54 mm	0.09	0.11	0.20	-0.37	4.04
			56 mm	0.03	0.11	0.14	-0.59	3.90
			58 mm	0.01	0.11	0.12	-1.23	3.25
			60 mm	0.01	0.11	0.12	-1.73	2.74

* Efficiency and sensitivity were normalized with those of a smooth hyperboloid.

to indicate that the scattered power does not contribute to further improvement of the efficiency, and we confirmed it through calculation of the illumination efficiency, i.e., by the integration with the amplitude and phase profile on the aperture. Even with other cones (curved cones of 48 to 52 mm in diameter), we have confirmed that the efficiency wasn't improved. When the efficiencies for the cones of 48 to 53 mm in diameter in Table 2 are set to zero, $\Delta\epsilon_{\text{ap}}/T$ is expected to be maximized with 53 mm cone and to achieve +4.47 % using the total spillover of the cone B, 0.169 %. Thus, the maximum $\Delta\epsilon_{\text{ap}}/T$ with the curved cone of 53 mm in diameter, +4.47 %, is almost equivalent to that with the straight cone of 52 mm in diameter, +4.53 % (the difference between them is 0.06 %).

Based on the above results, we have chosen the curved-shape cone of 53 mm in diameter, which is the maximum size to avoid the efficiency degradation even at 950 GHz and to maximize the sensitivity in the case of the curved cone².

4.2. Illumination profile and reflection coefficients at millimeter wavelengths

As described by Hills (2005), the illuminations on the Cassegrain focal plane and on the primary will have a lateral offset in cases of the offset feed. Thus, the offset feed might cause a strong reflection and a large spillover. However, if we can tilt the subreflector at a half angle of the feed tilt angle, it will help recover the suppression of the reflections. Radial distances of the ALMA front-end (FE) feeds from the primary axis and the tilt angles seen from the secondary are tabulated in Table 3. The maximum of the subreflector tilt angle to achieve the best performance is 2.04 degrees, which is larger than that used for the 12-m antenna,

² For reference, the best size to maximize the sensitivity at millimeter wavelength is summarized in Appendix B.

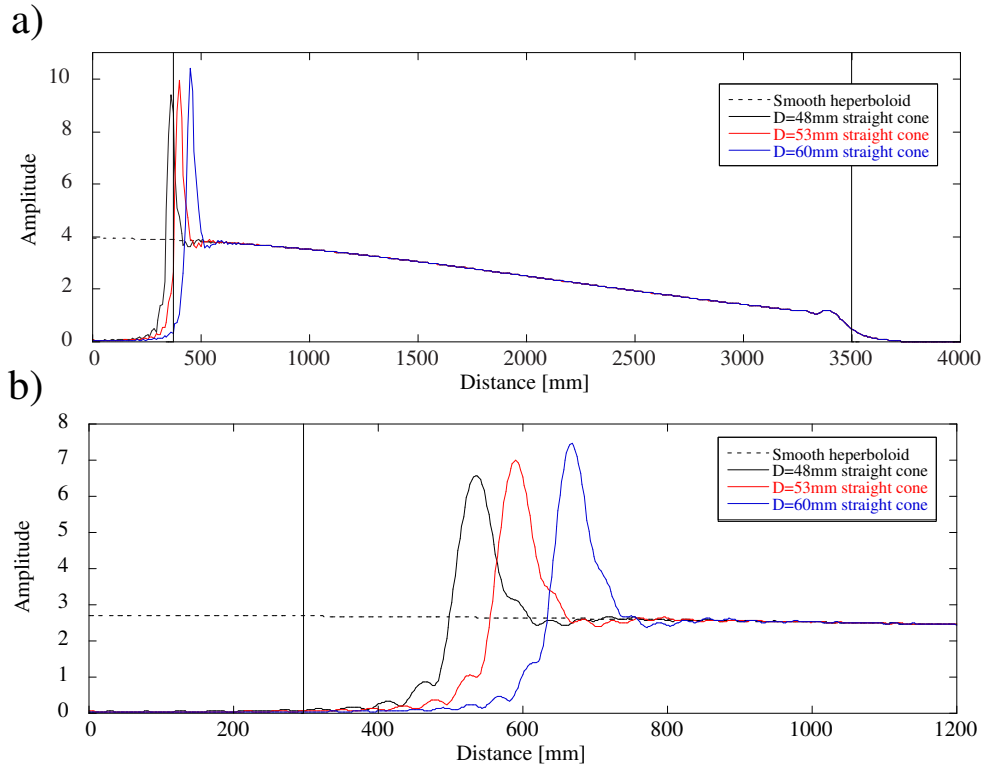


Fig. 8. (a) Illumination amplitude on the primary at 950 GHz. (b) The same as (a), but calculated on the Cassegrain focal plane.

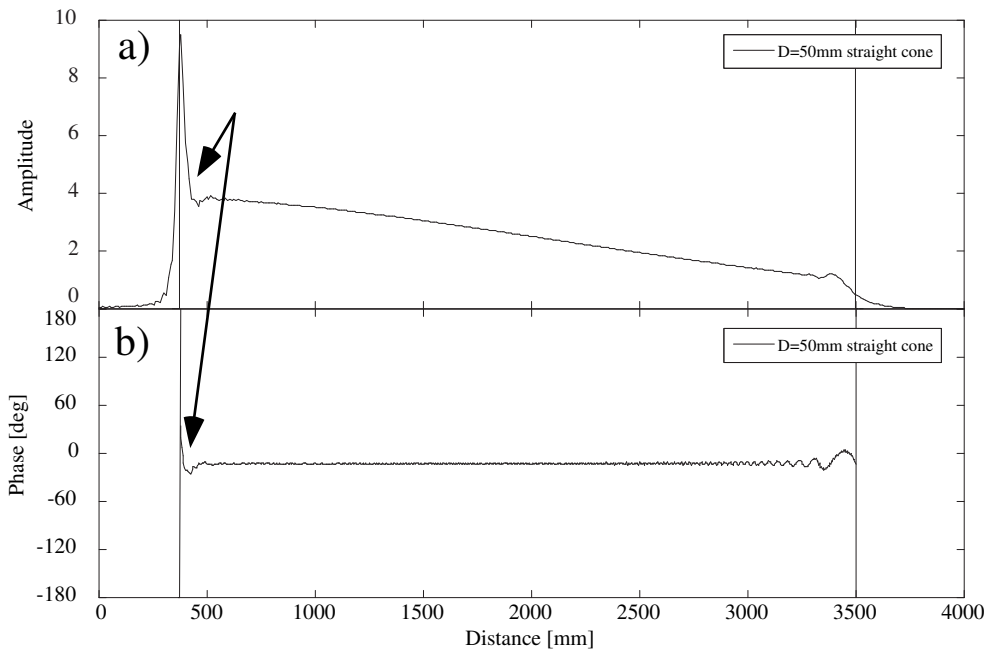


Fig. 9. (a) Illumination amplitude on the primary at 950 GHz with the straight cone of 50 mm in diameter. (b) The same as (a), but for the phase pattern on the aperture plane. The arrows indicate the additional efficiency contribution area.

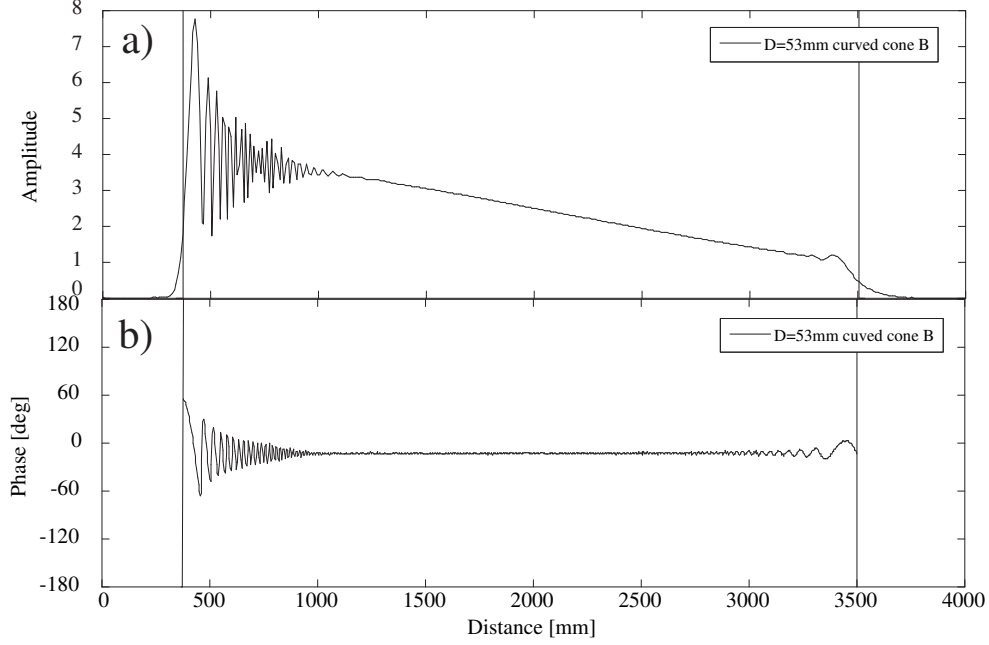


Fig. 10. (a) Illumination amplitude on the primary at 950 GHz with the curved cone B. (b) The same as (a), but for the phase pattern on the aperture plane.

Table 3. Off-axis feed and tilt angle

Band	1	2	3	4	5	6	7	8	9	10
Radius [mm]	255	255	188	194	245	245	100	103.3	100	100
Feed tilt [deg]	4.08	4.08	3.01	3.10	3.92	3.92	1.60	1.65	1.60	1.60
Needed subref tilt [deg]	2.04	2.04	1.50	1.55	1.96	1.96	0.80	0.83	0.80	0.80

1.215 degrees. The red values in Table 3 indicate the tilt angles larger than 1.215 degrees (Bands 1 to 6). The adjustment range is dependent on the size and detail structure of the subreflector adjustment mechanism. Therefore, the requirements of the angles larger than 1.215 degrees might be a challenge for the 7-m antenna design when we use the same type of the subreflector mechanism as the 12-m antenna. In the following study of the performance, we have compared cases with ideal/non-ideal subreflector tilt angles. The "non-ideal" subreflector tilt angle means 1.215 degrees, the maximum tilt angle for the subreflector of the 12-m antenna.

As we have already described in Section 3.2, the curved cone B is better for the case of offset feeds. Thus, we describe the reflection profiles with the curved cone B ($C = -0.62$, $D = -1.36$). Figures 11 – 14 show the illumination amplitude on the primary and on the Cassegrain focal plane at 84, 100, 163, and 211 GHz. Table 4 summarizes the reflection coefficients and the maximum peak-to-peak ripple based on the definitions in Section 3.3. In the Band 3 frequency range, the cone will reduce the reflection amplitude to the levels where $\eta_{\text{cone}} = 0.2$ to 0.1 of the

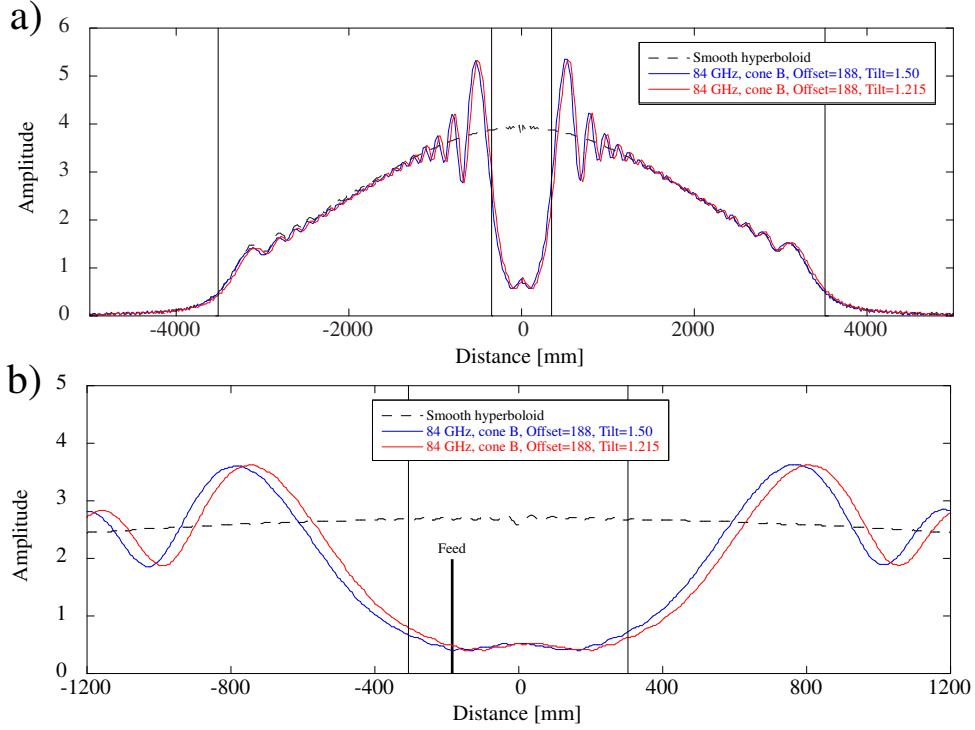


Fig. 11. Illumination amplitude with the feed 188 mm offset from the axis at 84 GHz. (a) On the primary (b) On the Cassegrain focal plane

case without the cone, and the difference between the cases with the "ideal" tilt (1.5 degrees) and the "non-ideal" tilt (1.215 degrees) is quite small. In the Band 5 – 6 frequency ranges, the difference becomes remarkable. For example, η_{cone} at the subreflector tilt of 1.215 degrees is 2 – 3 times higher than that at 1.96 degrees. However, η_{cone} and the ripple of the expected standing waves, $\Delta P/P$, are < 0.084 and < 0.07 %, which is still low even with the case of the "non-ideal" tilt.

We have calculated the effect of the tilt on the efficiency and the spillover at 211 GHz. The results are summarized in Table 5. The relative sensitivity, $\Delta\epsilon_{\text{ap}}/T$, was calculated on an assumption that a spillover of 1 % terminated at ambient temperature increases the system temperature by 5 %, which is a reasonable conversion for a system temperature of 50 K. As seen in Table 5, the spillover with the tilt of 1.96 degrees is back down to the very low figure of 0.7 % found for the on-axis case. Even when we compare the 1.215-degree tilt and 1.96-degree tilt, no fatal difference is found. For instance, the degradation levels of the spillover and the efficiency are ~ 0.3 % and ~ 0.1 %, respectively. The efficiency is however lower than the on-axis case by nearly 1.2 %. This is due to astigmatism caused by the tilt of the subreflector. Figure 15 describes the ray-tracing results for the efficiency loss. The frequency and the feed offset are 211 GHz and 245 mm. The black solid line indicates the efficiency loss due to the asymmetry of the illumination profile on the primary. Thus, that loss is maximized at the tilt

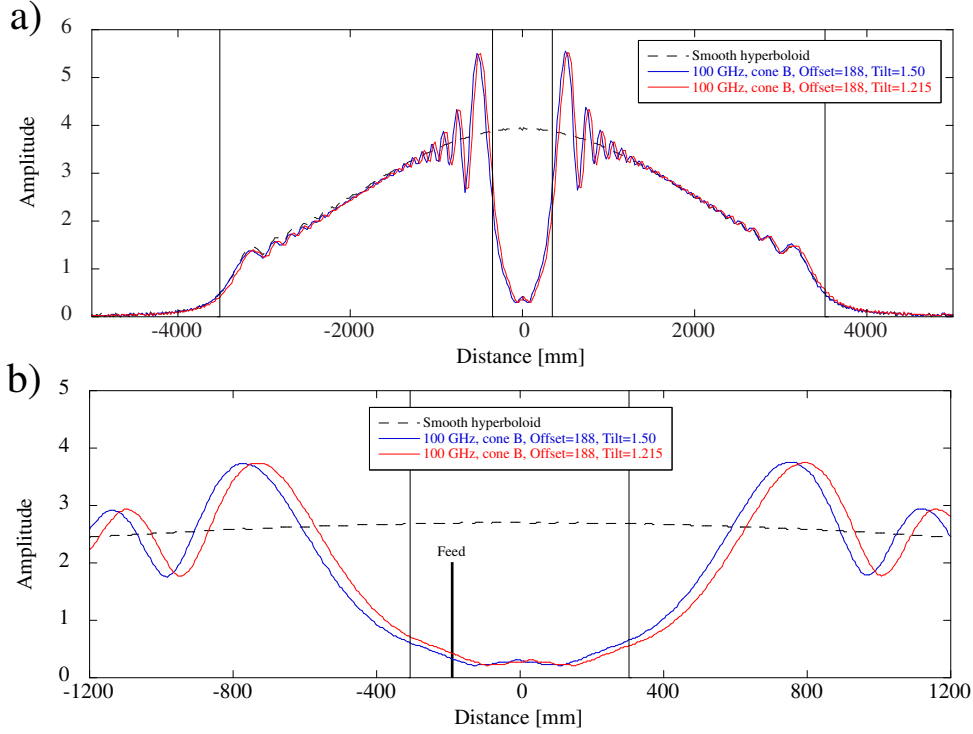


Fig. 12. Illumination amplitude with the feed 188 mm offset from the axis at 100 GHz. (a) On the primary (b) On the Cassegrain focal plane

of 0 degree and is minimized at the tilt of 1.96 degrees. The symmetry illumination is recovered at the 1.96-degree tilt. The black dashed line represents the phase loss. Even without the tilt, we see the loss of $\sim 0.3\%$, which is the contribution of the astigmatism by the feed offset (the curvature phase error was eliminated with a focal offset of the subreflector). As the subreflector tilt increases, the phase loss increases due to the astigmatism caused by the tilt. The blue line (total efficiency loss) shows the sum of the illumination loss and the phase loss. The loss of efficiency due to the astigmatism will be proportional to frequency squared and will reach close to 2.5% at the higher end of Band 6 (275 GHz). As all receivers for higher frequencies (Band 7 to 10) have small radial offsets (~ 100 mm), such effects will be smaller. According to the ray-tracing result, the 0.8% loss is estimated at 950 GHz with the 100 mm feed offset and the subreflector tilt angle of 0.8 degree.

We have to confirm other aspects like the effects of the asymmetry illumination and the phase error on the far-field beam patterns. Figures 16 – 18 describe the beam patterns when the subreflector is tilted at 0, 1.215, and 1.96 degrees. The beam patterns within the range of ± 0.2 degrees are displayed, which will be sufficient to see the above effects. In the case of 0 degree, we can see the asymmetry of the sidelobes in Figure 16 (a) and the asymmetry of the main beam in Figure 16 (b). The first sidelobe level is -23.1 dB below the peak of the main beam. In the case of the tilt of 1.215 degrees, the remarkable asymmetry of the sidelobes

Table 4. Reflection coefficient and peak-to-peak ripple in millimeter wavelengths with the curved cone B

Freq.	λ	w_0^*	Cone dia.	Cone shape	feed offset	Subref. tilt	Γ_{s0}	η_{cone}	Γ_s	Γ_f	$\Delta P/P$
[GHz]	[mm]	[mm]	[mm]		[mm]	[deg]					[%]
84	3.57	20.79	None	–	0	0.000	9.34e-3	1.000	9.34e-3	0.4	1.49
			53	curved cone B	188	1.215		0.184	1.72e-3	0.4	0.27
			53	curved cone B	188	1.500		0.150	1.40e-3	0.4	0.22
100	3.00	17.49	None	–	0	0.000	7.87e-3	1.000	7.87e-3	0.4	1.26
			53	curved cone B	188	1.215		0.158	1.25e-3	0.4	0.20
			53	curved cone B	188	1.500		0.121	9.50e-4	0.4	0.15
163	1.84	10.76	None	–	0	0.000	4.85e-3	1.000	4.85e-3	0.4	0.78
			53	curved cone B	245	1.215		0.084	4.06e-4	0.4	0.07
			53	curved cone B	245	1.960		0.046	2.24e-4	0.4	0.04
211	1.42	8.32	None	–	0	0.000	3.75e-3	1.000	3.75e-3	0.4	0.60
			53	curved cone B	245	1.215		0.054	2.01e-4	0.4	0.03
			53	curved cone B	245	1.960		0.018	6.82e-5	0.4	0.01

* Gaussian with a -12 dB edge taper and with $R = L_f$ at the subreflector edge was assumed.

Table 5. Efficiency and spillover with the curved cone B at 211 GHz

Freq. [GHz]	Feed offset [mm]	Tilt of subref [deg]	Cone dia. [mm]	Spillover total [%]	$\Delta\epsilon_{\text{ap}}$ [%]*	$\Delta\epsilon_{\text{ap}}/T$ [%]*
211	On axis	None	None	3.67	0.00	0.00
	On axis	None	53	0.69	0.59	18.18
	245	None	None	4.21	-2.86	-5.39
	245	None	53	1.26	-3.33	9.91
	245	1.215	None	3.72	-1.53	-1.77
	245	1.215	53	0.98	-1.17	14.23
	245	1.96	None	3.66	-1.60	-1.53
	245	1.96	53	0.70	-1.08	16.20

* The curved cone's efficiency and sensitivity were normalized with those of a smooth hyperboloid. The focal position of the subreflector was adjusted in order to reduce the phase error caused by the feed offset and maximize the efficiency. The focus displacements from the nominal position are +0.5, 0.3, and 0.18 mm for the subreflector tilts of 0, 1.215, and 1.96 degrees.

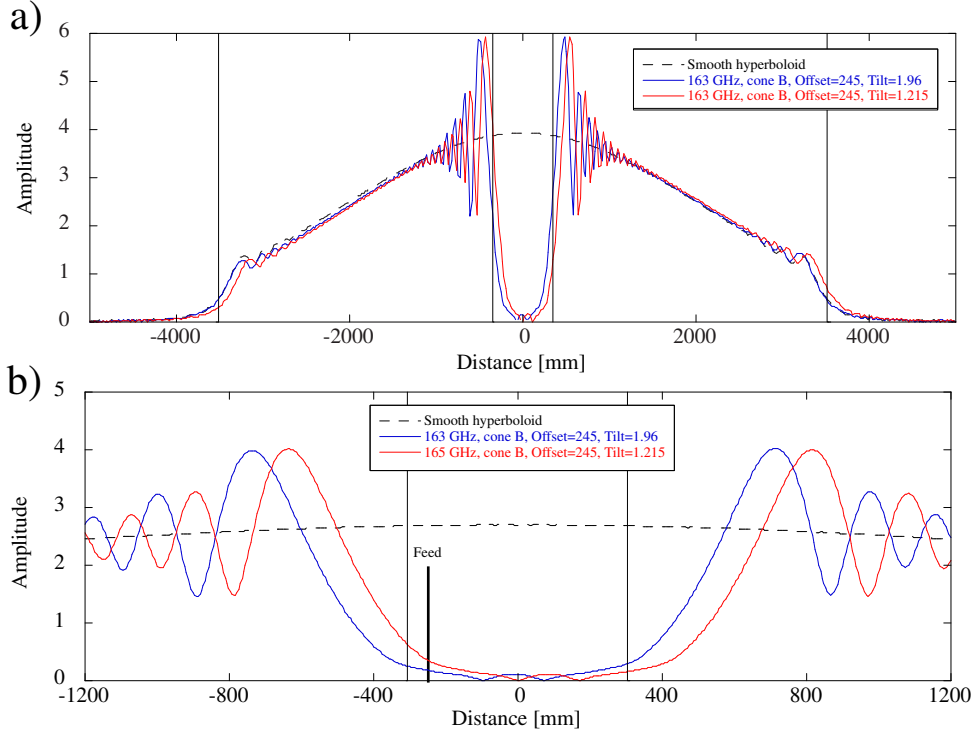


Fig. 13. Illumination amplitude with the feed 245 mm offset from the axis at 163 GHz. (a) On the primary (b) On the Cassegrain focal plane

disappears and the symmetry of the main beam can be recovered above -15 dB. However, the phase error by the tilt increases the first sidelobe level (-22.1 dB below the peak). In the case of the tilt of 1.96 degrees, the symmetry of the main beam seems to reach above -20 dB, however the first sidelobe becomes higher (~ -21 dB).

The beam pattern with the curved cone B is shown in Figure 19. The feed is on the axis here for simplicity. Since we performed PO with rough grids to reduce the calculation time, Figure 19 shows almost no sharp diffraction patterns. However, the effect of the cone can be seen clearly. We see that the energy scattered by the cone is spreading over a wide range of angles, up to about ~ 1.3 degrees. Since the main beam peak gain is about 82 dBi at this frequency, the diffuse component is below the peak level by the order of 60 dB, which is unlikely to cause any undesirable consequences.

4.3. Conclusions

We have designed the central cone for the subreflector of the ACA 7-m antenna. The cone diameter is set to 53 mm to avoid the efficiency degradation even at 950 GHz as well as to suppress the reflected field on the Cassegrain focal plane. The cone will be slightly curved in order to minimize the reflection for the offset feed. The optimum set of parameters defined in the equation (1) for the curved-shape cone is $C = -0.62$, $D = -1.36$. To evaluate the benefit of the cone quantitatively, we have calculated the amplitude profiles on the Cassegrain focal

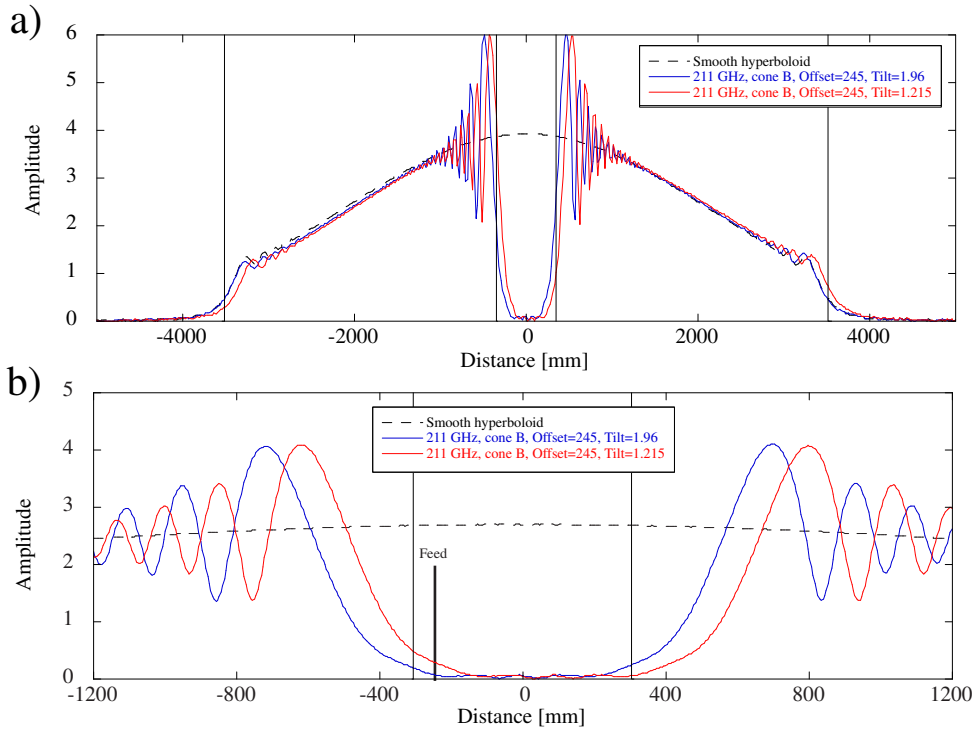


Fig. 14. Illumination amplitude with the feed 245 mm offset from the axis at 211 GHz. (a) On the primary (b) On the Cassegrain focal plane

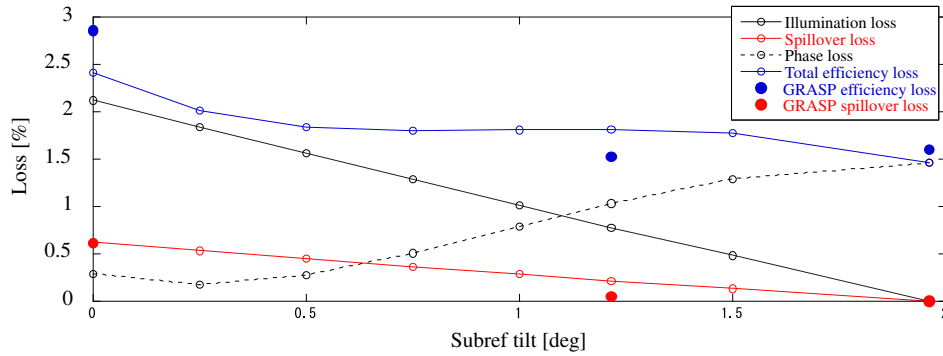


Fig. 15. Efficiency and spillover when the subreflector is tilted without the cone. The frequency and the feed offset are 211 GHz and 245 mm. The loss is normalized with that of the on-axis case. The black solid and dotted lines indicate the illumination and phase loss calculated by the ray-tracing. The blue line is the sum of them. The red line indicates the spillover calculated by the ray-tracing. Filled circles indicate the results of GRASP tabulated in Table 5.

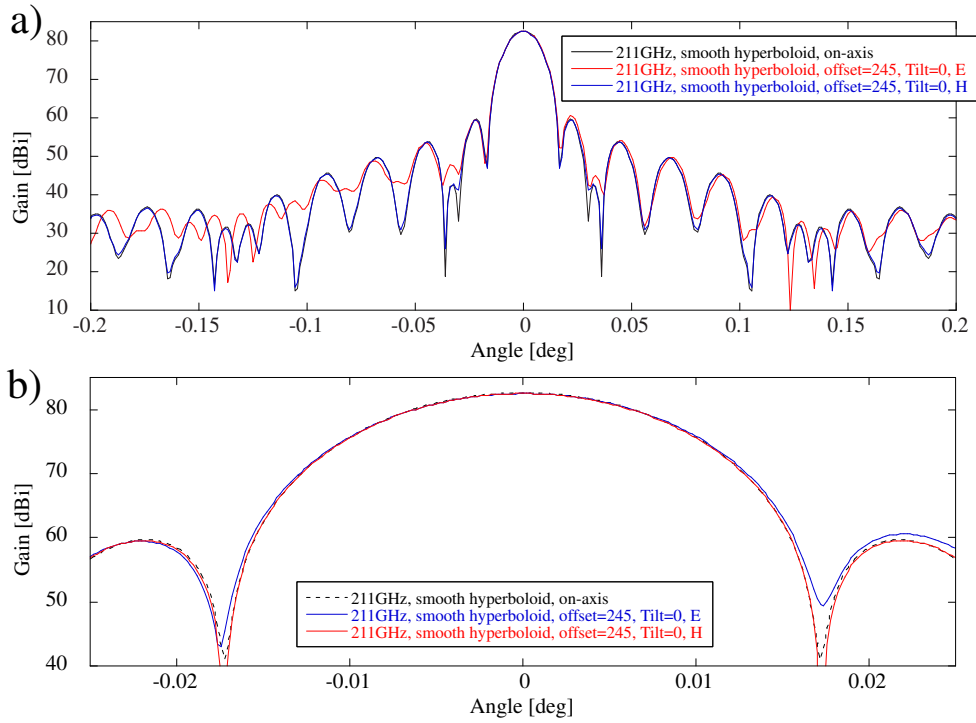


Fig. 16. 211-GHz beam patterns with the subreflector tilt of 0 degree. Pointing offsets were eliminated.

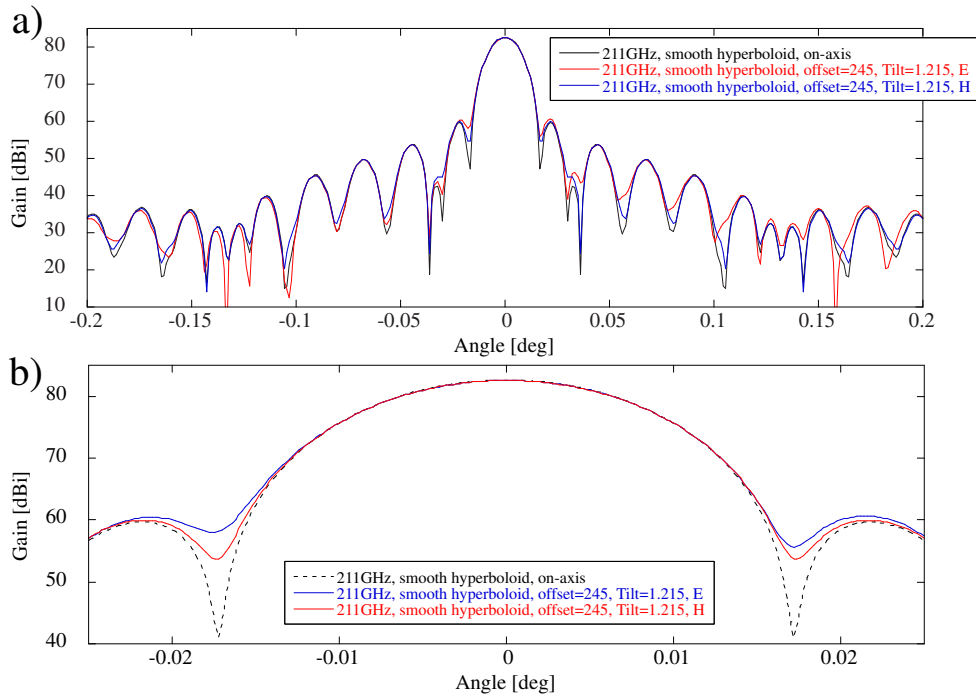


Fig. 17. 211-GHz beam patterns with the subreflector tilt of 1.215 degrees.

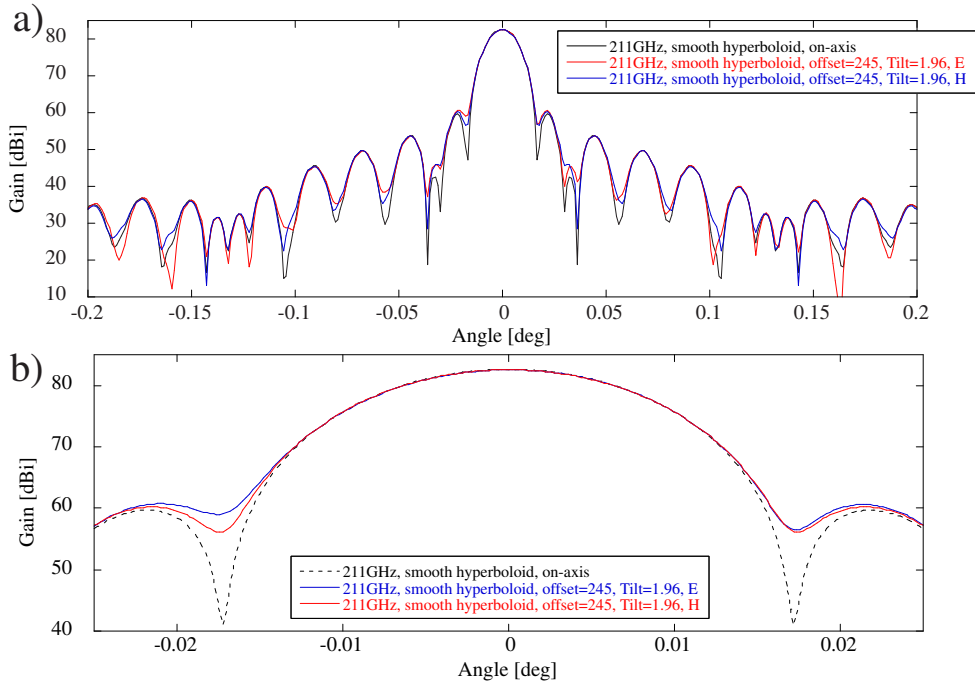


Fig. 18. 211-GHz beam patterns with the subreflector tilt of 1.96 degrees.

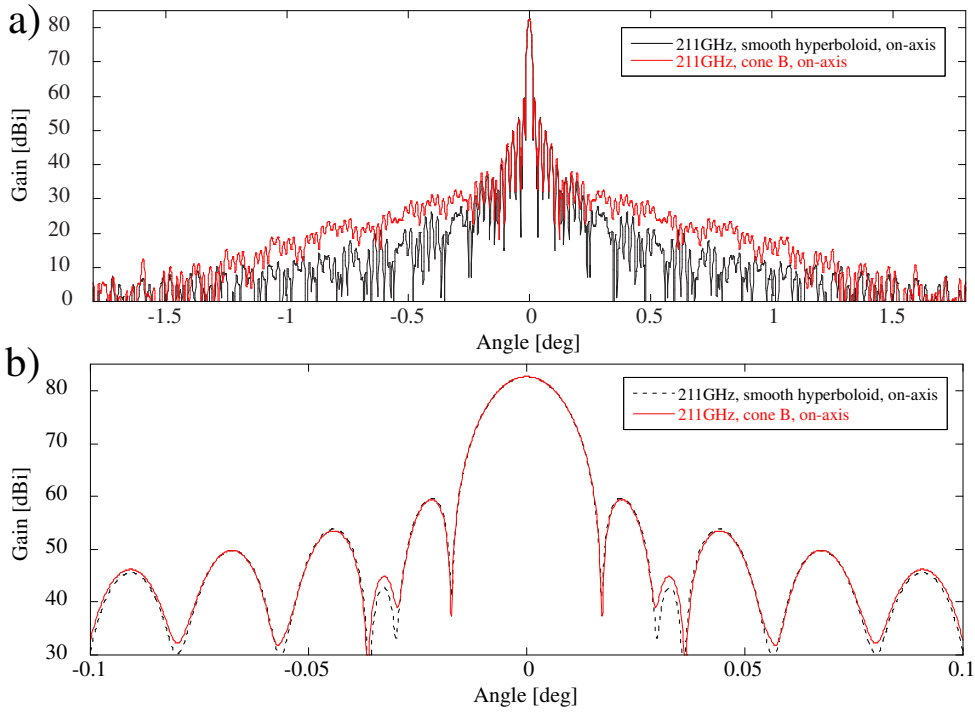


Fig. 19. Far-field beam pattern with the cone B at 211 GHz.

plane with and without the cone, and compared the power contributions to the standing waves in these cases. The reflected power is more reduced with the cone than without the cone. The ratio of the reflected power to the nominal power in the Cassegrain focal plane, $\Delta P/P$, is found to be 0.15–0.3 % in the Band 3 frequency range (84 and 100 GHz), and 0.01–0.07 % at the lower end frequencies of Band 5 and 6. The far-field beam patterns with the cone will have high sidelobes over ± 1.3 degrees, however, the power level is 60 dB below the peak gain of the main beam.

We compared the cases of the "non-ideal" subreflector tilt (1.215 degrees) and the "ideal" tilt through the calculation of the various performances. The performance degradation caused by the "non-deal" tilt seems to be an acceptable level.

References

- Baars, J. W. M. 2000, ALMA memo 339
 Bacmann, A. and Guilloteau, S. 2003, ALMA memo 457
 Goldsmith, P. F. 1998, Quasioptical Systems (New York: IEEE Press)
 Hills R. 1986, Memo ASR/MT/T/1015
 Hills R. 2005, ALMA memo 545
 Lamb, J. W. 1999, ALMA memo 246
 Lucke, R. L., Fischer, J., Polegre, F. A., and Beintema, D. A., 2005, Applied Optics, 44, 5947-5955
 Morita, K.-I., & Holdway, M. 2005, ALMA memo 538
 Morris, D. 1978, A&A, 67, 221-228
 Pety, J., Gueth, F., & Guilloteau, S. 2001, ALMA memo 398
 Padman, R. and Hills, R. 1991, Int. J. Infrared Millim. Waves, 12, 589-599
 Tsutsumi, T., Morita, K.-I., Hasegawa, T., & Pety, J. 2004, ALMA memo 488
 Zhang X. 1996, SMA technical memo, No. 85

Appendix A – The spillover effect on G/T

System noise temperature can be written as

$$T_{\text{sys}} = \frac{\exp(\tau_0 \cdot \sec Z)}{\eta_{\text{ant}}} \cdot [T_{\text{rx}} + T_{\text{amb}}(1 - \eta_{\text{ant}}) + T_{\text{atm}}(1 - \exp(-\tau_0 \cdot \sec Z))\eta_{\text{ant}}], \quad (7)$$

where τ_0 , $\sec Z$, η_{ant} , T_{rx} , T_{amb} , T_{atm} , are zenith optical depth, air mass at zenith distance, antenna efficiency, receiver noise temperature, ambient temperature, and sky temperature, respectively. If we assume $\tau_0 \cdot \sec Z = 1$, $\eta_{\text{ant}} = 0.95$, $T_{\text{rx}} = 230$ K, $T_{\text{amb}} = T_{\text{atm}} = 300$ K, $T_{\text{sys}} = 1217$ K is derived. In case of $\eta_{\text{ant}} = 0.94$, T_{sys} is 1233 K. Thus if the η_{ant} is changed by 1 % when $T_{\text{sys}} = 1200$ K, T_{sys} is changed by 1.3 % accordingly.

Table 6. Gain and spillover with the straight cones at 100 and 200 GHz.

Frequency [GHz]	Offset in focal plane	Tilt of subref	Cone diameter	Spillover [%]	$\Delta\epsilon_{\text{ap}}$ [%]*	$\Delta\epsilon_{\text{ap}}/T$ [%]*
100	On axis	None	None	3.83	0.00	0.00
			48 mm	2.50	1.20	8.40
			52 mm	1.99	1.13	11.36
			54 mm	1.73	1.20	13.04
			55 mm	1.61	1.22	13.86
			60 mm	1.06	1.16	17.39
			65 mm	0.77	0.84	19.04
			70 mm	0.58	-0.16	19.22
			75 mm	0.55	-1.33	17.97
200	On axis	None	None	3.68	0.00	0.00
			48 mm	2.36	0.72	7.84
			52 mm	1.49	0.97	13.39
			54 mm	1.10	0.97	15.91
			55 mm	0.94	0.93	16.97
			60 mm	0.46	0.23	19.48
			65 mm	0.39	-0.69	18.86
			70 mm	0.37	-1.95	17.48
			75 mm	0.36	-2.93	16.40

* Gain and sensitivity were normalized with those of a smooth hyperboloid.

Appendix B – Cone size optimization at millimeter wavelengths

We calculated the efficiency and spillover for the straight cones in the various sizes at millimeter wavelengths. Table 6 indicates the calculation results of the efficiency and the spillover for the straight cones. The sensitivity was calculated on an assumption that a spillover of 1 % terminated at ambient adds 5 % to the system temperature, which is about right for a system temperature of 50 K.

As the 7-m antenna has the large ratio of the vertex hole size to the primary as described in Section 2, the efficiency is expected to improve by 17 – 20 % by introducing the cone. This improvement rate is more significant than the 12-m antenna case which is 4 – 5 %. In this estimation, we assumed that all power passing through the vertex hole are terminated at ambient temperature. This might lead to overestimation, however, it is clear that the central cone has large contributions not only to the suppression of the standing waves but also to noise reduction. With regard to the sensitivity at around 100 – 200 GHz, the optimum size of the cone diameter is 60 to 70 mm.